4. F.G. Perey and B. Buck, Nucl. Phys. **32**, 353 (1962).
5. E.J. Stephenson, R.C. Johnson, J.A. Tostevin, V.R. Cupps, J.D. Brown, C.C. Foster, J.A. Gering, W.P. Jones, D.A. Low, D.W. Miller, H. Nann, C. Olmer, A.K. Opper, P. Schwandt, J.W. Seubert, and S.W. Wissink, Phys. Lett. B **171**, 358 (1986).
6. E.J. Stephenson, R.C. Johnson, and J.A. Tostevin, contribution to this report.

NATURE OF THE MISSING NEAR-SIDE AMPLITUDE IN CALCULATIONS OF INTERMEDIATE ENERGY (d,p) AND (p,d) REACTIONS

E.J. Stephenson

Indiana University Cyclotron Facility, Bloomington, Indiana 47405

R.C. Johnson and J.A. Tostevin

University of Surrey, Guildford, Surrey GU2 5XH, United Kingdom

Model calculations of the cross section and analyzing powers for (d,p) and (p,d) transfer reactions at energies near 100 MeV often bear little resemblance to the measured angular distributions. To provide a basis for a detailed investigation, cross section and analyzing power angular distributions have been made for two time-reverse pairs of reactions, ^{116}Sn(d,p)^{117}Sn with ^{117}Sn(p,d)^{116}Sn (Refs. 1 and 2) and ^{66}Zn(d,p)^{67}Zn and ^{67}Zn(p,d)^{66}Zn (presented elsewhere in this report). These studies find the greatest problems for $j_n = \ell_n - \frac{1}{2}$ transitions, where the presence of a marked interference pattern in the analyzing power angular distributions indicates nearly equal contributions to the reaction amplitude from the far and near sides of the nucleus.[4] In distorted wave Born approximation calculations there is almost no near-side contribution, and the model angular distributions show almost no interference pattern. We have continued to investigate this issue using semi-classical reaction analysis techniques with the intention of extracting a phenomenological extimate of the size and character of the missing near-side amplitude. The data for this investigation come from the $\ell_n = 4, j_n = \frac{7}{2}$ transition in ^{116}Sn(d,p)^{117}Sn.

A semi-classical analysis of the reaction amplitudes may be pursued in this case for two reasons. First, the typical deuteron and proton partial waves that contribute to the stripping or pick-up amplitude are large enough that semi-classical approximations are a useful representation of the reaction. Second, the dynamics of angular momentum matching at the nuclear surface have sufficiently strong effects that only a few of the possible amplitudes contribute significantly to the reaction. This leads in the case of the model calculations to redundancy relations among the polarization observables which are not matched by experiment.[4]

In Fig. 1a, this dynamic selectivity picks out one projection (λ_n) of the transferred neutron's orbital angular momentum. In a model calculation (without spin-orbit distortions for simplicity), this is the maximal projection normal to the asymptotic reaction plane with the sense of rotation commensurate with far-side scattering. Since this is a
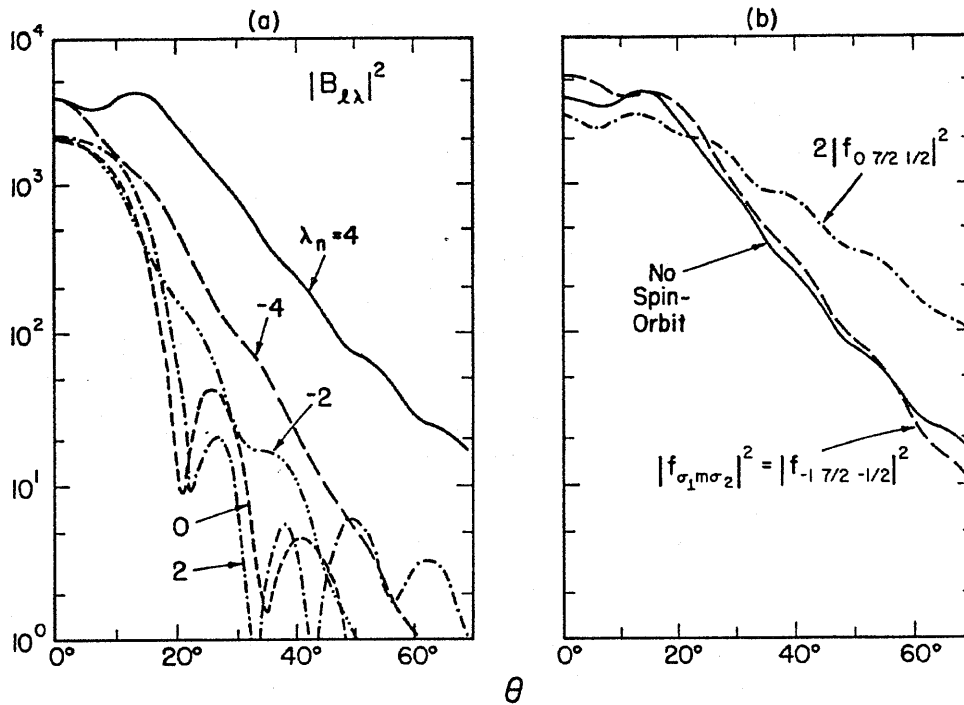
Figure 1. (a) Angular distributions of the absolute squares of the reaction amplitudes for the five allowed projections of the transferred angular momentum, $\lambda_n = 4$, 2, 0, -2, and -4. This model calculation is zero range (no deuteron D-state) and has no spin-orbit distortions. (b) Angular distributions of the absolute squares of reaction amplitudes where $\lambda_n = 4$. The "no spin-orbit" case is repeated from Fig. 1a, the new curves with spin-orbit distortions correspond to deuteron and proton projection quantum numbers of $(\sigma_1, \sigma_2) = (0, \frac{1}{2})$ and $(-1, -\frac{1}{2})$.

$j_n = \ell_n - \frac{1}{2}$ transition, there is likewise only one projection (m_n) for the total angular momentum (j_n) for which the amplitude is large, the maximal one $(m_n = 7/2)$. If we quantize along an axis normal to the plane, the Bohr rule requires that the deuteron and proton spin projections (σ_1 and σ_2) obey the relation

$$\sigma_2 - \sigma_1 = \ell_n - m_n = \frac{1}{2} \tag{1}$$

Thus only two paris of values, $(\sigma_1, \sigma_2) = (0, \frac{1}{2})$ and $(-1, -\frac{1}{2})$, are allowed for the spin projection quantum numbers. Fig. 1b shows that even with spin-orbit distortions, both of these amplitudes remain large. Their difference attests to the strength of the spin-orbit distortions.

By looking at the partial reaction cross sections for each projection of the deuteron spin, we may select these amplitudes individually for study. Fig. 2 shows measurements corresponding to the three partial cross sections

$$(d\sigma/d\Omega)_1 = (d\sigma/d\Omega)(\frac{1}{3} + \frac{1}{2}A_y + \frac{1}{6}A_{yy})$$

$$(d\sigma/d\Omega)_0 = (d\sigma/d\Omega)(\frac{1}{3} - \frac{1}{3}A_{yy}) \tag{2}$$

$$(d\sigma/d\Omega)_{-1} = (d\sigma/d\Omega)(\frac{1}{3} - \frac{1}{2}A_y + \frac{1}{6}A_{yy})$$

along with full model calculations. These calculations include adiabatic deuteron distorted waves, exact finite range with the deuteron D-state, and non-locality corrections. The potential parameters are taken from Ref. 1. Both $(d\sigma/d\Omega)_0$ and $(d\sigma/d\Omega)_{-1}$ show interference oscillations not present in the calculations, and $(d\sigma/d\Omega)_1$ is substantially underestimated.
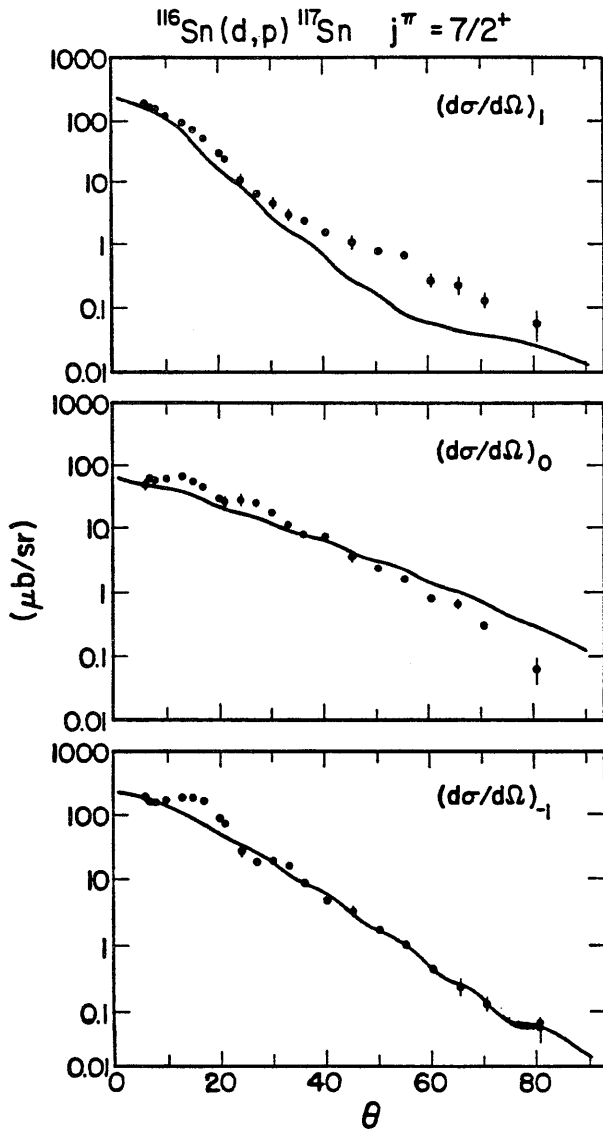

Figure 2. Angular distributions of the three deuteron spin projection partial cross sections compared with full model calculations.

112

Since the model amplitudes represent a strongly surface-peaked reaction, they may be replaced in a semi-classical approximation by a resonance in partial wave number. For this purpose we chose the form

$$R(\ell_2) = R_0 \, \text{sech}^2\left(\frac{\ell_2 - L}{2\Delta}\right) \qquad (3)$$

which is written as a resonance in terms of the proton partial wave number (ℓ_2). For simplicity in this investigation, the resonance parameters $(R_0, L, \text{ and } \Delta)$ were adjusted to reproduce the ℓ_2-dependence of the largest radial integral contributing to each partial cross section. The spin coupling for each obeyed the constraint implied by Eg. (1), and was:

$$\text{For } (d\sigma/d\Omega)_0, \quad R_{\ell_2 j_2 \ell_1 j_1} = R_{\ell_2, \ell_2 + \frac{1}{2}, \ell_2 + 4, \ell_2 + 4} \qquad (4)$$

$$\text{For } (d\sigma/d\Omega)_{-1}, \quad R_{\ell_2 j_2 \ell_1 j_1} = R_{\ell_2, \ell_2 - \frac{1}{2}, \ell_2 + 4, \ell_2 + 3} \qquad (5)$$

The parameters for these fits are given in Table I. The reproduction of the surface resonance for both cases is shown in Fig. 3.
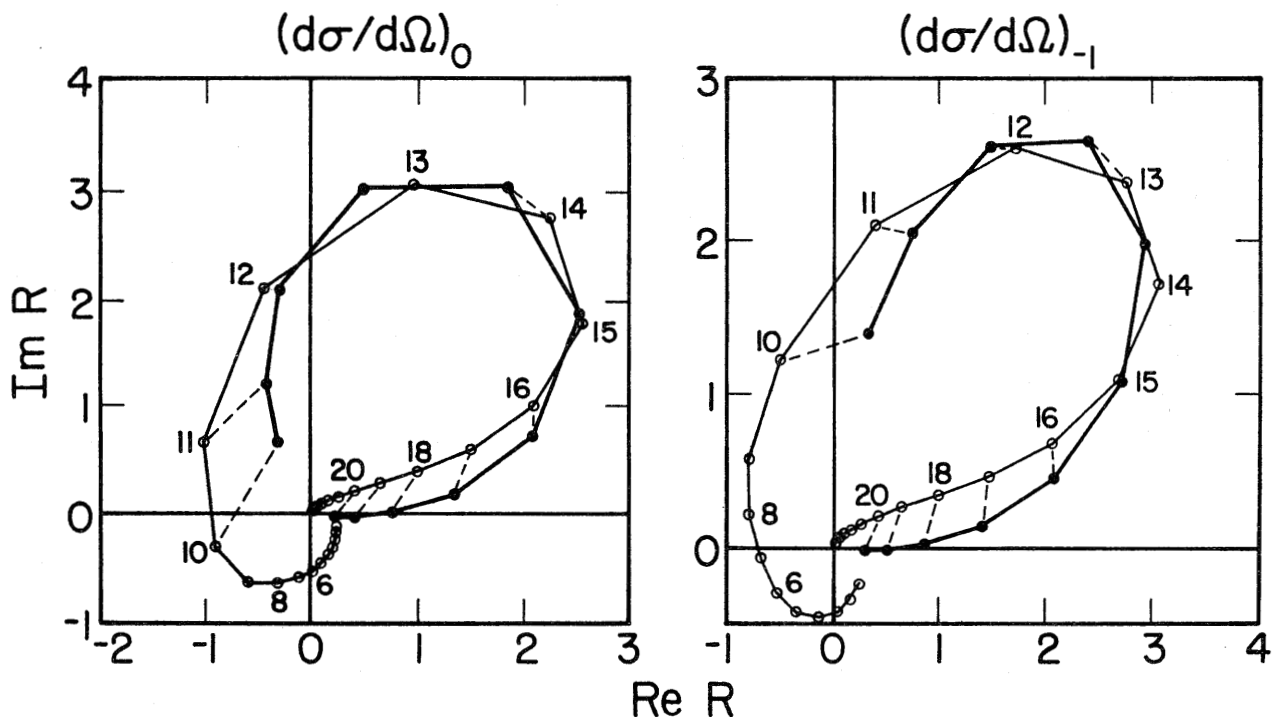

Figure 3.   Argand diagrams showing the amplituded associated with the $\sigma_1 = 0$ partial cross section (a) and the $\sigma_1 = -1$ partial cross section (b). The solid line connects values associated with the best-fit resonance formula.

Table I: Parameters for the Semi-Classical Model Resonances.

	$(d\sigma/d\Omega)_0$	$(d\sigma/d\Omega)_{-1}$
R_o	$1.37 + 2.15i$	$2.30 + 2.03i$
L	$14.05 - 1.78i$	$13.46 - 1.42i$
Δ	1.58	1.78
$\pi\Delta + L_I$	3.17	4.16
α	3.55	4.36

A near-side/far-side decomposition of the radial integrals in Eqs. (4) and (5) shows that their contributions to $(d\sigma/d\Omega)_0$, and $(d\sigma/d\Omega)_{-1}$, comes only from their far-side pieces. (For this to be strictly true for $(d\sigma/d\Omega)_0$, we must in addition assume that the dominant amplitude is $\langle \sigma_2 M \mid T \mid \sigma_1 \rangle = \langle \frac{1}{2}, \frac{7}{2} \mid T \mid 0 \rangle$.) For an interference pattern to exist, a near-side amplitude of comparable size must exist. Information concerning this amplitude comes from the quantum numbers of that amplitude and the sizes obtained form adjusting it to reproduce the measurements. This latter analysis assumes that the partial cross sections are the result of interference between two surface-peaked resonances. The measurements of $(d\sigma/d\Omega)_0$, and $(d\sigma/d\Omega)_{-1}$, were reproduced by a formula involving two interfering single-pole resonances. In such a fit, the near-side and far-side character of the resonances is lost. Afterward, the resonance whose parameters match the model resonance is assumed to be far-side, and the remaining set is associated with the missing near-side amplitude.

The form of Eq. (3) contains both near-side and far-side pieces (as it must to reproduce a real model radial integral). In the fit, we used a single-pole form to represent the pole of Eq. (3) closest to the real axis

$$R(\ell_2) = R_0 \left(\frac{-i\frac{\Delta}{2}}{\ell_2 - L - i\frac{\Delta}{2}} \right)^n \tag{6}$$

The form used to reproduce $(d\sigma/d\Omega)_0$, and $(d\sigma/d\Omega)_{-1}$, was

$$\sin\theta \left(\frac{d\sigma}{d\Omega} \right) = A^2 \theta^{2(m-1)} e^{-2\alpha\theta} + (a^2 + \bar{a}^2)\theta^{2(n-1)} e^{-2\beta\theta}$$

$$+ 2A\theta^{m-1}\theta^{n-1} e^{-(\alpha+\beta)\theta} [a\cos(t\theta) + \bar{a}\sin(t\theta)] \tag{7}$$

where an overall phase has been removed, making A real. The orders of the two poles are m and n, their widths are α and β, and the period of interference pattern is governed by $t = L(1) + L(2)$. The nearest pole of Eq. (3) is second-order ($n = 2$). Fits were attempted for all orders (values of m and n). Starting values were chosen so that $\alpha > \beta$, thus insuring that most of the large angle cross section (ascribed to the far-side amplitude) would be reproduced by the first term in Eq. (7). A sensitivity to order was observed only for the

first term, with $(d\sigma/d\Omega)_0$ preferring $m = 2$ and $(d\sigma/d\Omega)_{-1}$ preferring $m = 1$. To obtain a useful comparison with the resonance parameters of Eq. (3), we chose the fit where $m = n = 2$ in both cases. These fits are shown in Fig. 4 and the parameters of Eq. (7) listed in Table II. The correspondence of the two resonant forms Eqs. (3) and (6) requires
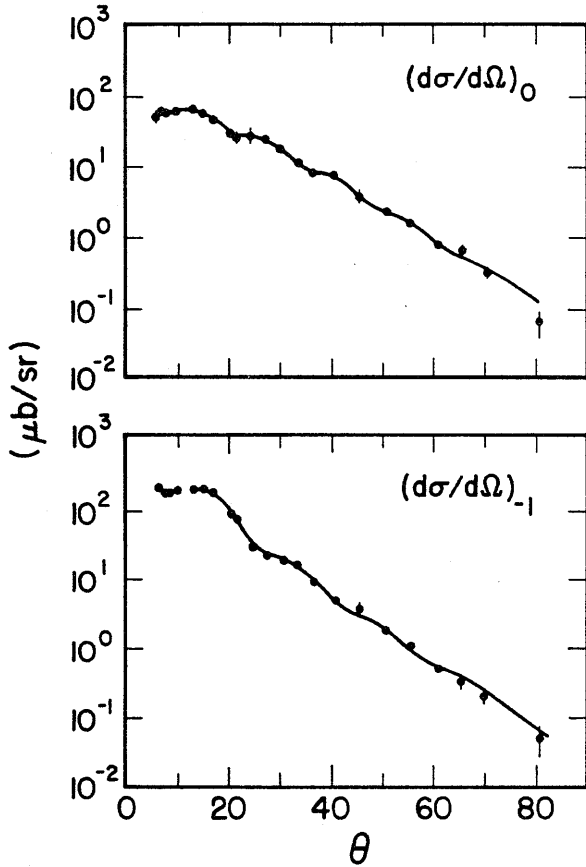
$$\alpha = \pi\Delta + L_I \tag{8}$$

Figure 4. Measurements of the $\sigma_1 = 0$ and $\sigma_1 = -1$ partial cross sections, together with the fitted double-resonance formula shown over the angular range where data was included. The forward angle $\sigma_1 = -1$ points were omitted.

Table II. Double Resonance Parameters.

	$(d\sigma/d\Omega)_0$	$(d\sigma/d\Omega)_{-1}$
A	35.36 ± 0.80	57.8 ± 4.7
a	3.5 ± 1.2	219 ± 121
$\bar{a}$	0.0 ± 1.6	$-32. \pm 67$
α	3.549 ± 0.035	4.36 ± 0.13
β	4.05 ± 0.61	11.1 ± 1.5
t	26.04 ± 0.75	$2\,0.0 \pm 1.0$
χ^2/ν	1.7	4.7

115

where L_I is the imaginary part of L. The comparison of these quantities for the resonance underlying the first term of Eq. (7) is given in Table I, and supports the association of these amplitudes.

While both near-side and far-side pieces are needed to fully describe the amplitude missing from the model calculations, we may examine the size of the contribution from the single near-side pole of Eq. (7) assuming that it represents the bulk of the amplitude. For the $(d\sigma/d\Omega)_{-1}$ case, the far-side portion of the missing amplitude will contribute to $(d\sigma/d\Omega)_1$. Assuming that all of the difference between the model calculation and the data for $(d\sigma/d\Omega)_1$ is attributed to this term, an additional contribution of only 10% is obtained. Figure 5 shows Argand plots of the two model amplitudes described by
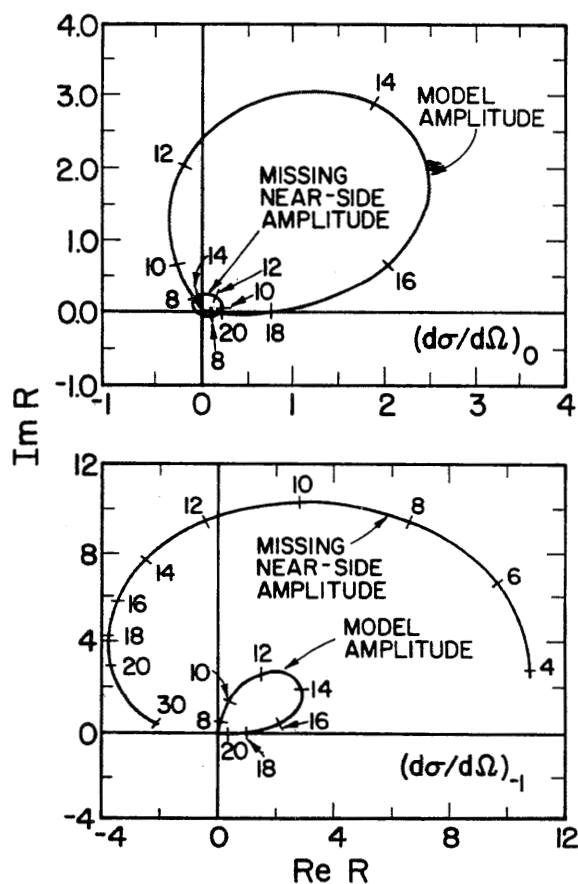

Figure 5. Argand plots of the model amplitudes and missing near-side amplitudes for $(d\sigma/d\Omega)_0$ and $(d\sigma/d\Omega)_{-1}$. The number denote partial wave in the proton channel.

Eq. (3). In addition, the missing near-side resonances of Eq. (7) are shown. For $(d\sigma/d\Omega)_0$ the additional piece is small while for $(d\sigma/d\Omega)_{-1}$ it is substantially larger than the model amplitude. The size of these terms rests entirely on the a and $\bar{a}$ coefficients of Table II. since it is only the size of the interference pattern that determines these coefficients, large uncertainties result. In addition, the missing amplitude for $(d\sigma/d\Omega)_{-1}$ is large over a broad range of partial waves, and these tend to cancel in the sum leading to the calculated cross section. Despite these uncertainties, it is clear that a near-side amplitude comparable

116

in size to the far-side amplitude from the model can be generated that will explain the interference pattern.

Additional information concerning the missing, near-side dominated amplitude may be obtained from the spin coupling for its associated matrix element. For interference to occur in the $(d\sigma/d\Omega)_{-1}$ case, where this amplitude is the largest, the radial matrix element associated with that in Eq. (5) becomes

$$\text{For near side} \quad (d\sigma/d\Omega)_{-1}, \quad R_{\ell_2 j_2 \ell_1 j_1} = R_{\ell_2, \ell_2 + \frac{1}{2}, \ell_2 - 4, \ell_2 - 3} \tag{9}$$

Its largest values appear for $\ell_2 = 6.5$ (this value is determined by the difference $t - L$). Because of the coupling in Eq. (9), this corresponds to a peak in deuteron partial wave near $\ell_1 = 2.5$, a central collision. The picture obtained from this amplitude is that of a head-on collision between the deuteron and the nucleus that gives rise to back-to-back neutron-proton separation with the proton emerging on the near side. The sense of rotation in the neutron orbit must be the same as for the far-side amplitude, or else the two pieces will not add coherently as needed to generate an interference pattern.

One reason this near-side amplitude is missing from our standard reaction model involves the large relative n-p momentum present at the scission point. For the far-side contribution, $k_{np} \sim 0.6$ fm^{-1}, a value still within range of the bound-state deuteron internal momentum. That this value is large indicates that even for $\ell = 4$ transfer, the neutron does not have enough angular momentum in the bound state to make this reaction well-matched in angular momentum at the nuclear surface. For the near-side amplitude, the relative momentum must increase to $k_{np} \sim 1.3$ fm^{-1}. The smallness of the bound-state deuteron wavefunction for this value of k_{np} insures that it will be negligable in a distorted wave model. One possible explanation that is under investigation is the inclusion of break-up through a coupled-channel calculation, with the hope that the intermediate breakup state would have sufficient strength at larger values of k_{np}. In a recently published review, Yahiro shows momentum distributions for breakup into relative S- and D-waves (see Fig. 16 of Ref. 5). While the D-wave distribution peaks between $k_{np} = 0.3$ and 0.4 fm^{-1}, it too is essentially zero by $k_{np} = 1.3$ fm^{-1}. Additional calculations are being made with the hope that higher internalk angular momentum states may prove to be the appropriate intermediate step.

1. V.R. Cupps, J.D. Brown, C.C. Foster, W. P. Jones, D.W. Miller, H. Nann, P. Schwandt, E.J. Stephenson, and J.A. Tostevin, Nucl. Phys. **A469**, 445 (1987).
2. E.J. Stephensson, V.R. Cupps, J.A. Tostevin, R.C.Johnson, J.D. Brown, C.C. Foster, W.P. Jones, D.W. Miller, H. Nann, and P. Schwandt, Nucl. Phys. **A469**, 467 (1987).
3. E.J. Stepheson, A.D. Bacher, G.P.A. Berg, V.R. Cupps, D.A. Low, D.W. Miller, C. Olmer, A.K. Opper, B.K. Park, R. Sawafta, and S.W. Wissink, contribution to this report.
4. E.J. Stephenson, R.C. Johnson, J.A. Tostevin, V.R. Cupps, J.D. Brown, C.C. Foster, J.A. Gering, W.P. Jones, D.A. Low, D.W. Miller, H. Nann, C. Olmer, A.K. Opper, P. Schwandt, J.W. Seubert, and S.W. Wissink, Phys. Lett. B **171**, 358 (1986).
5. M. Yahiro, Y. Iseri, H. Kameyama, M. Kamimura, and M. Kawai, Prog. Theo. Phys. Suppl. **89**, 32 (1986).